INVESTIGATING THE INFLUENCE OF CERTAIN PARAMETERS ON THE DYNAMIC CHARACTERISTICS OF A COMPOSITE WING STRUCTURE

Marwa L. Agela and Gamal M. Ashawesh

Aeronautical Engineering Department, Faculty of Engineering, University of Tripoli, Libya.

E-mail: marwaagela@gmail.com

Received 30 July 2024, revised 8 September 2024, accepted 26 September 2024

الملخص

تناقش هذه الورقة تأثير بعض العوامل مثل اتجاهات الألياف وتسلسل تكديس الصفائح ونسب الأبعاد وصلابة نماذج صندوق الجناح المستطيل المركب لتحليل الاهتزاز الحر على تكوينين للجناح، الأول ينتج اقتران ماديا وصلابة الانحناء والالتواء والآخر بدون اقتران مادي، تتلاشى صلابة الانحناء والالتواء. تم تطوير برنامج كمبيوتر ضمن لغة MATLAB للتعامل مع حساب صلابة الانحناء والالتواء والانحناء-الالتواء (EI,GJ,K) لتكوينين للجناح من أجل فهم سلوكهما. يتم إجراء تحليل الاهتزاز الحر أيضًا باستخدام برنامج العناصر المحدودة MSC / PATRAN و / MSC NASTRAN v2004 لنفس تكوينات الجناح. تم العثور على أقصى صلابة للانحناء وصلابة الالتواء وصلابة اقتران الانحناء والالتواء عند اتجاهات الألياف 0° و±30° و±20° على التوالي لـ CAS ومع اقتران صفري لنماذج CUS. وقد وجد أن صلابة الجناح تتناسب بشكل عالميا مع نسب العرض إلى الارتفاع. لوحظت اختلافات مماثلة في صلابة المواد والترددات الطبيعية وأشكال الأنماط مقابل زوايا الألياف. إن تأثير نسبة العرض الى الارتفاع على تردد الانحناء الأساسي يكاد يكون مهملاً مقارنة بتردد الالتواء، في حين أن تأثير K أكثر وضوحًا على تردد الالتواء مقارنة بتردد الانحناء.

ABSTRACT

This paper discusses the effect of some parameters such as fibre orientations, laminate stacking sequence, aspect ratios and stiffness of the rectangular composite wing box models for the free vibration analysis on two wing configurations, the first one producing a material coupling, bend-twist stiffness and the other without material coupling, bend-twist stiffness vanishes. A computer program within MATLAB language is developed to deal with the calculation of the bending, torsion and bend-twist stiffnesses (EI, GJ, and K) for the two wing configurations in order to understand their behaviour. Free vibration analysis is also carried out using the finite element program MSC/PATRAN and MSC/NASTRAN v2004 for the same wing configurations. The maximum bending stiffness, torsion stiffness and bend-twist coupling stiffness are found at 0º, ±30 º and ±20 º fibre orientations respectively for the CAS and with zero coupling for the CUS models. It was found that wing stiffnesses are universally proportional with the aspect ratios. A similar variations of the material stiffnesses, eigenvalues and associated eigenvectors versus fibre angle are observed. The effect of aspect ratio on the fundamental bending frequency is almost negligible compared with the torsional frequency, whereas K is more pronounced on the torsional frequency compared with bending frequency.

KEYWORDS: Stiffnesses; Composite Material; Fibre Orientations; Free Vibration.

INTRODUCTION

Aircraft designers frequently strive for lighter parts, which leads to flexible structures that are more susceptible to distortion from loads. The lifting surface structures' shape is primarily responsible for aerodynamic loads. These loads will result in completely different aerodynamic loads if they in any way alter the geometry and produce deformations in the structure. The relationship between inertia, stiffness, and aerodynamic forces is categorized as AEROELASTICITY [1]. As illustrated in Figure (1) below, Collar's triangle of forces can be used to categorize a variety of aeroelastic phenomena. The triangle's vertices are home to three different kinds of forces: (i) aerodynamic forces; (ii) elastic forces; and (iii) inertial forces. Mechanical vibrations result from the interaction of inertial and elastic forces, and this relationship is crucial for the analytical solution of dynamic aeroelastic problems. This means that while designing an aircraft, consideration of vibration characteristics in the form of eigenvalues and eigenvectors is crucial to preventing dynamic aeroelastic instabilities like flutter. Because composite materials perform better, they are being used more frequently in real-world applications, such as automobile and aerospace structures. This is primarily because composite materials offer high stiffness to weight and high strength to weight ratios. The desire for a deeper comprehension of composite material vibration properties is motivated by the growing requirement for lightweight aircraft structures. This understanding is crucial for the analysis of dynamic aeroelastic instabilities. Numerous research works have examined the vibration and flutter analysis of cantilevered composite aircraft wings, which closely resemble the fuselage-wing connection found in real aircraft. Among the earlier research are, free vibration of a thin-walled laminated composite beam is examined by Vo, T. P. et al., [2]. The equations of motion for the analytical model come from Hamilton's principle, while the classical lamination theory serves as its foundation. Finite element analysis was used to calculate natural frequencies and mode shapes. The numerical results demonstrated how the vibration analysis was affected by the fibre angle, modulus ratio, and boundary conditions. Khan, J. Z. [3] studied of thin-walled constructions' static and dynamic behaviour, both theoretical and experimental. For structural idealization, the dynamic stiffness matrix technique is employed. The study conducted by Ovesy et al., [4] examined the free vibration behaviour of thin-walled composite box beams. It was conducted by taking into account various assumptions in the constitutive equations. Some non-classical effects, like transverse shear and restricted warping, are included in the current model. The dynamic stiffness matrix approach, which was introduced by Banerjee, J. et al. [5], is an exact analytical technique for figuring out the free vibration properties of simple or composite beams. The effects of warping, rotating inertia, and shear deformation were disregarded in this work. Sari, B. et al. [6] studies examine composite tapered aircraft wing structures using ANSYS Workbench and CATIA. Examining the impact of winglets on natural frequencies, it is discovered that winglets lower the natural frequency of carbon epoxy UD shell material, which is higher than that of kevlar epoxy. Clydin, P. A. et al. [7] study the free vibration characteristics of laminated composite box sections using Finite Element Software ANSYS 15, determining natural frequencies and analysing the variation of these frequencies with the proposed design parameter. Hortaa, T.B. et al. [8] analyse free vibration of laminated composite beam problems using Timoshenko beam finite elements and examine parasitic shear effects in natural frequencies and mode shapes computation.

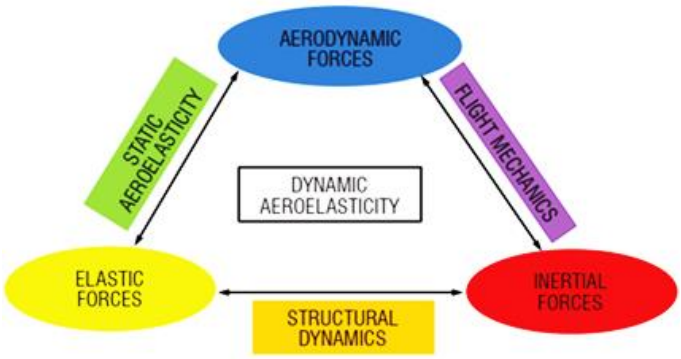

Figure 1: Collar's aero-elastic triangle [1].

STIFFNESS OF COMPOSITE WING SECTION

Materials and Methods

As a first step, understanding the behaviour and variation of the stiffnesses of the composite material, a computer program using MATLAB is developed according to the formulation presented in [9] to calculate the wing box stiffnesses. Two case studies, wing 1 and wing 3 models are tested using the two configurations (CAS and CUS) shown in Figures (2) and (3) below.

The equations for calculation of effective stiffness EI, GJ and K are derived from Chandra et al. Ref. [9]. These equations are to be read in conjunction with Figure (4).

$$EI = \sum_{p=1}^{n} \iint_{1,2} \bar{C}_{11}^{k} z^2 dydz + \sum_{p=1}^{m} \iint_{3,4} \bar{C}_{11}^{k} z^2 dydz \quad (1)$$

$$GJ = \sum_{p=1}^{n} \iint_{1,2} \bar{C}_{33}^{k} \hat{z}^2 dydz + \sum_{p=1}^{m} \iint_{3,4} \bar{C}_{33}^{k} \hat{y}^2 dydz \quad (2)$$

$$K = \sum_{p=1}^{n} \iint_{1,2} \bar{C}_{13}^{k} \hat{z}\, z dydz \quad (3)$$

The (1, 2) denote the top and bottom skin laminates of the box-beam, respectively. and (3,4), respectively, stand for the box-beam's left and right skin laminates. Where:

$$\bar{C}_{11} = q_{11} - \frac{q_{12}^2}{q_{22}}$$

$$\bar{C}_{13} = q_{13} - \frac{q_{12} \times q_{23}}{q_{22}}$$

$$\bar{C}_{33} = q_{33} - \frac{q_{23}^2}{q_{22}}$$

$$\hat{z} = z + \lambda,\ y \text{ and } \hat{y} = y - \lambda,\ z$$

$$\lambda = \left(\frac{c-d}{c+d}\right) yz$$

Where q_{11}, q_{12}, q_{22}, q_{13}, q_{23}, and q_{33} are found through the matrix shown below:

$$\begin{bmatrix} q_{11} \\ q_{22} \\ q_{33} \\ q_{12} \\ q_{13} \\ q_{23} \end{bmatrix} = \begin{bmatrix} m^4 & n^4 & 2m^2n^2 & 4m^2n^2 \\ n^4 & m^4 & 2m^2n^2 & 4m^2n^2 \\ m^2n^2 & m^2n^2 & -2m^2n^2 & (m^2-n^2)^2 \\ m^2n^2 & m^2n^2 & m^4+n^4 & -4m^2n^2 \\ m^3n & -mn^3 & mn^3-m^3n & 2(mn^3-m^3n) \\ mn^3 & -m^3n & m^3n-mn^3 & 2(m^3n-mn^3) \end{bmatrix} \begin{bmatrix} Q_{11} \\ Q_{22} \\ Q_{12} \\ Q_{33} \end{bmatrix}$$

$$Q_{11} = {}^{E_1}/_{(1 - v_{12}v_{21})}$$

$$Q_{12} = {}^{v_{21}\,E_1}/_{(1-v_{12}v_{21})}$$

$$Q_{22} = {}^{E_2}/_{(1-v_{12}v_{21})}$$

$$Q_{33} = G_{12}$$

The variables n and m represent the number of layers in laminates 1 and 2, and 3 and 4, respectively. The coordinates in the cross-sectional plane are y, z. $\boldsymbol{\lambda}$ represents the torsion warping function, c the beam's chord, and d its depth. Transformed reduced stiffness is denoted by q_{ij} where θ is ply orientation, $m = \cos(\theta)$ and $n = \sin(\theta)$.

The computer program is validated with Ref. [9], the results of symmetric top and bottom $(0°/90°)_3$ and symmetric right and left $(0°/90°)_3$ laminate lay-ups are presented in Table (1).

Table 1: Comparison of *EI*, *GJ* and *K* for Ref. [9].

Stiffness	Present MATLAB programming results	Ref. [9]	Error in (%)
EI (Ib.in^2)	44.351×10^3	45×10^3	1.44%
GJ (Ib.in^2)	8.0008×10^3	8.0×10^3	-0.01%
K (Ib.in^2)	0	0	0.0%

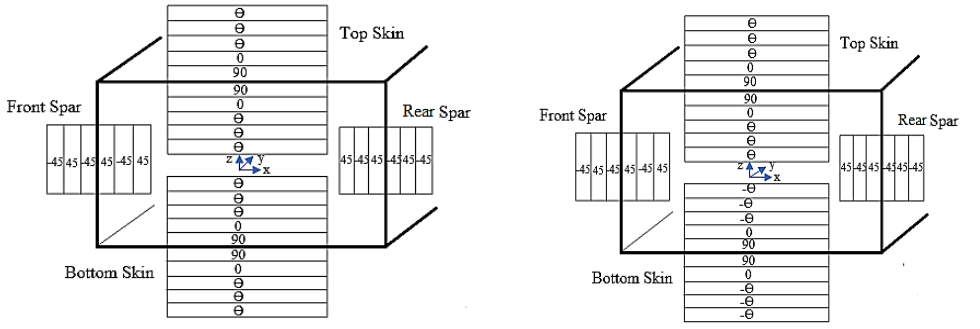

Wing 1 model Wing 2 model

Figure 2: Circumferentially Asymmetric Stiffness (CAS) configuration of the wing 1 model and Circumferentially Uniform Stiffness (CUS) configuration of the wing 2 model

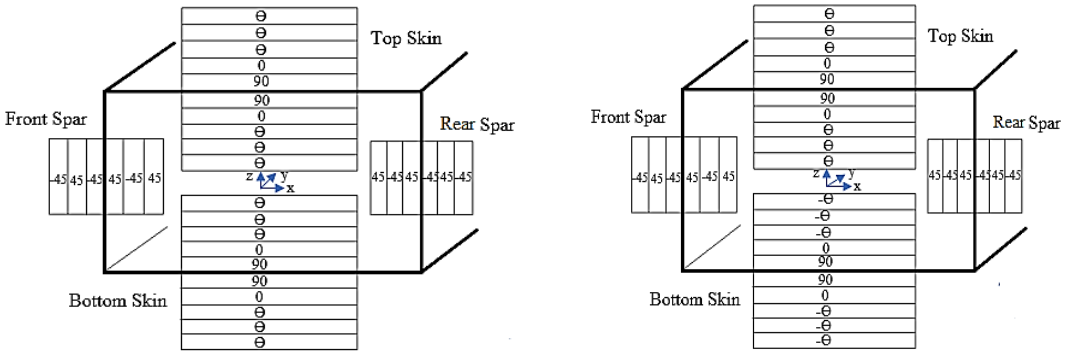

Wing 3 model Wing 4 model

Figure 3: Circumferentially Asymmetric Stiffness (CAS) configuration of the wing 3 model and Circumferentially Uniform Stiffness (CUS) configuration of the wing 4 model.

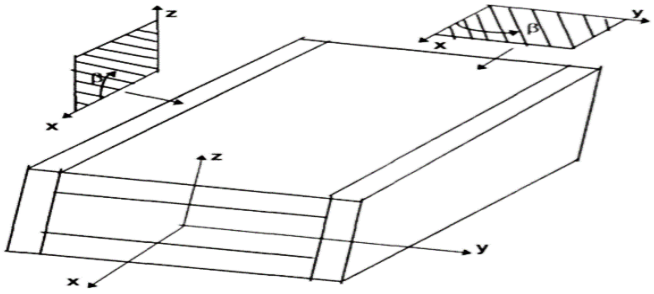

Figure 4: Box-beam configuration and coordinate [10].

After validation of the developed program, four wing models are constructed, the first wing box (wing 1 consists of the skins, front and rear spars. The laminate lay-up is used $(\theta_3/0°/90°)_s$ for the skins, where θ is the most outer ply angle in the laminates stacking sequence and it was oriented over the range $-90° \leq \theta \leq 90°$. The web sides are made from antisymmetric laminate $(\pm 45°)_3$ to avoid the bend-twist coupling produced by the side webs as shown in Figure (2). The third wing box structure (wing 3) is similar to the wing 1 model, but with different laminate. The laminate lay-up is used $(90°/0°/\theta_3)_s$ for the upper and the lower skins, where θ is the most inner ply angle in the laminates stacking sequence and it was oriented over the range, $-90° \leq \theta \leq 90°$. The web sides are made from antisymmetric laminate $(\pm 45°)_3$ as shown in Figure (3). The material properties used for two thin-walled structures, wing 1 and wing 3 are given in the Table (2). The stiffness properties in terms of bending stiffness EI, torsion stiffness GJ, and bend-twist coupling K for wing 1 and wing 2 models are shown in table (3) and Figures (5) and (6). For wing 3 and wing 4 models, bending stiffness EI, torsion stiffness GJ, and bend-twist coupling K are presented in Table (4) and Figures (7) and (8).

Table 2: Ciba-Geigy 913 Carbon/Epoxy prepreg properties, thin-walled

Property	Value
E_1 (N/m^2)	130×10^9
E_2 (N/m^2)	9×10^9
υ_{12}	0.28
G_{12} (N/m^2)	4.8×10^9
ρ (kg/m^3)	1.6×10^3
Ply thickness (m)	0.17×10^{-3}
Depth (m)	13×10^{-3}
Width (m)	35×10^{-3}
Length (m)	0.762

The maximum value of the bending stiffness EI is found at fibre orientation, $\theta = 0°$. This value falls off rapidly with a small change in fibre orientation for laminate lay-up. The lower resistance is offered in the transverse direction at $\theta = \pm 90°$. The torsion stiffness GJ has the maximum value at $\theta \cong \pm 30°$ for the laminate lay-up as shown in Figure (5), whereas the lower values of torsional stiffness are found at $\theta = 0°$ and $\theta = \pm 90°$.The bend-torsion coupling K is fully antisymmetric with the fibre angle $\theta = 0°$ respect to a reference axes direction as shown in Figure (5). The K is maximum at fibre angle $\theta \cong \pm 20°$. At fibre orientations of 0º and ±90º, the bend-torsion coupling K, is zero. The bending–torsion stiffness ratio $EI/_{GJ}$ is fully symmetry about the fibre angle

zero degree as shown in Figure (6). The maximum value of the bending–torsion stiffness ratio $^{EI}/_{GJ}$ is in the fibre direction θ = 0°. This value falls off rapidly with a small change in fibre orientation for the laminate lay-up. The lower resistance is offered in the transverse direction at $\theta \cong \pm 45°$, due to the lower value of bending stiffness and higher value of torsional stiffness. Finally, the parameter $^{K}/_{GJ}$ is fully antisymmetric with the fibre angle $\theta = 0°$ respect to a reference axes direction as shown in Figure (6). The parameter $^{K}/_{GJ}$ is maximum at fibre angle $\theta \cong \pm 15°$. The lowest resistance is offered in the transverse direction when $\theta = 0°$ and $\theta = \pm 90°$.

For the wing 2 model (CUS), bending-torsion coupling vanishes, ($k = 0$), that is due to the effects of opposite sign of fibre angle θ for both sides (upper & lower and left & right), thus k value canceled each other due to the sign effect. The bending stiffness, torsion stiffness and bending-torsion stiffness ratio are the same as CAS composite configuration.

Table 3: Stiffnesses and stiffnesses ratio of wing 1 model.

Θ	EI (N.m^2)	GJ (N.m^2)	K (N.m^2)	EI/GJ	K/GJ
0°	411.94	64.040	0	6.43	0
±15°	356.16	95.845	±84.300	3.72	±0.880
±30°	217.74	117.51	±67.4	1.85	±0.574
±45°	151.24	95.005	±23.946	1.59	±0.252
±60°	136.06	76.150	±6.358	1.79	±0.0835
±75°	133.26	66.793	±1.218	2.00	±0.0182
±90°	132.90	64.040	0	2.08	0

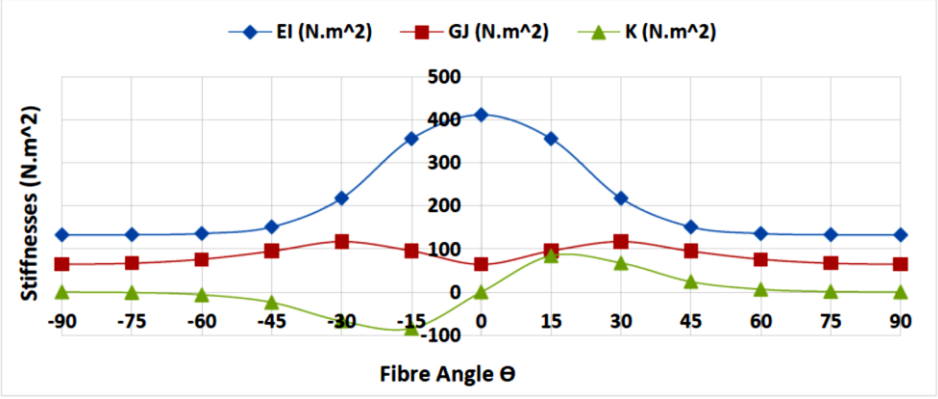

Figure 5: Stiffnesses verse fiber angle Θ, wing 1 model.

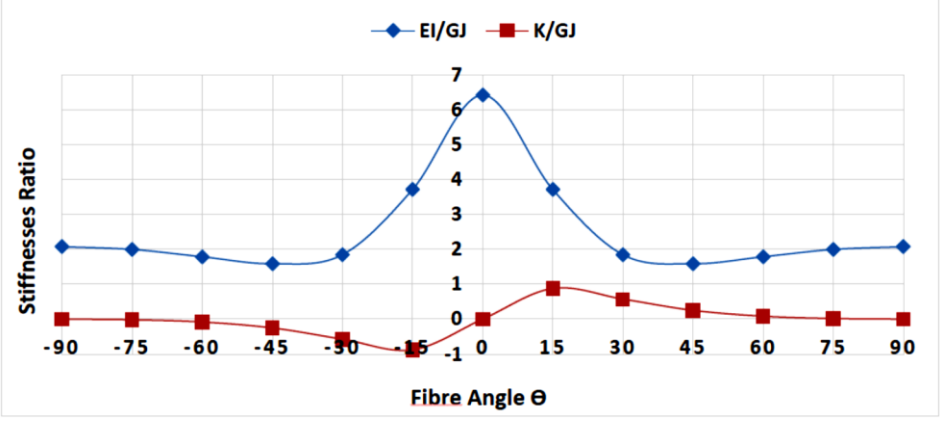

Figure 6: Stiffnesses ratio verse fiber angle Θ, wing 1 model.

The bending stiffness EI is symmetrical about the zero-fibre angle θ as shown in Figure (7). The maximum value of the bending stiffness EI is the in-fibre direction, $\theta = 0°$. The lowest resistance is offered in the transverse direction at $\theta = \pm 90°$. The torsion stiffness GJ has the maximum value at $\theta \cong \pm 30°$ for the laminate lay-up as shown in Figure (7). Also, the least resistance is offered at $\theta = 0°$ and $\theta = \pm 90°$.The bending-torsion coupling stiffness K is fully antisymmetric with the fibre angle $\theta = 0°$ respect to a reference axes direction as shown in Figure (7). The is maximum at fibre angle $\theta \cong \pm 20°$. The bend-torsion coupling, K is vanishing at fibre angle of $\theta = 0°$ and $\theta = \pm 90°$.The bending –torsion stiffness ratio $^{EI}/_{GJ}$ is fully symmetry about the fibre angle θ respect to a reference axes direction as shown in Figure (8). The maximum value of the bending –torsion stiffness ratio $^{EI}/_{GJ}$ is the in-fibre direction θ = 0°. This value falls off rapidly with a small change in fibre orientation for the laminate lay-up. The lower resistance is offered in the transverse direction at $\theta \cong \pm 45°$. Finally, the parameter $^{K}/_{GJ}$ is fully antisymmetric with the fibre angle $\theta = 0°$ respect to a reference axes direction as shown in Figure (8). The parameter $^{K}/_{GJ}$ is maximum at fibre angle $\theta \cong \pm 15°$. It vanishes at $\theta = 0°$ and $\theta = \pm 90°$.

The upper and lower flanges of the wing 4 model are made of the identical laminate lay-up, but with the fibre angle θ reversed, as seen in Figure (3). The bending stiffness, torsion stiffness, and bending-torsion stiffness ratio of the wing 3 CAS composite design will all be the same in this arrangement, and there won't be a bending-torsion coupling (k = 0).

Table 4: Stiffnesses and stiffnesses ratio of the wing 3 model.

Θ	EI (N.m^2)	GJ (N.m^2)	K (N.m^2)	EI/GJ	K/GJ
0°	410.27	64.041	0	6.41	0
±15°	354.99	95.561	±83.545	3.71	±0.874
±30°	217.81	117.03	±66.820	1.86	±0.571
±45°	151.91	94.728	±23.732	1.60	±0.251
±60°	136.86	76.042	±6.301	1.80	±0.0829
±75°	134.09	66.768	±1.208	2.010	±0.0181
±90°	133.73	64.041	0	2.090	0

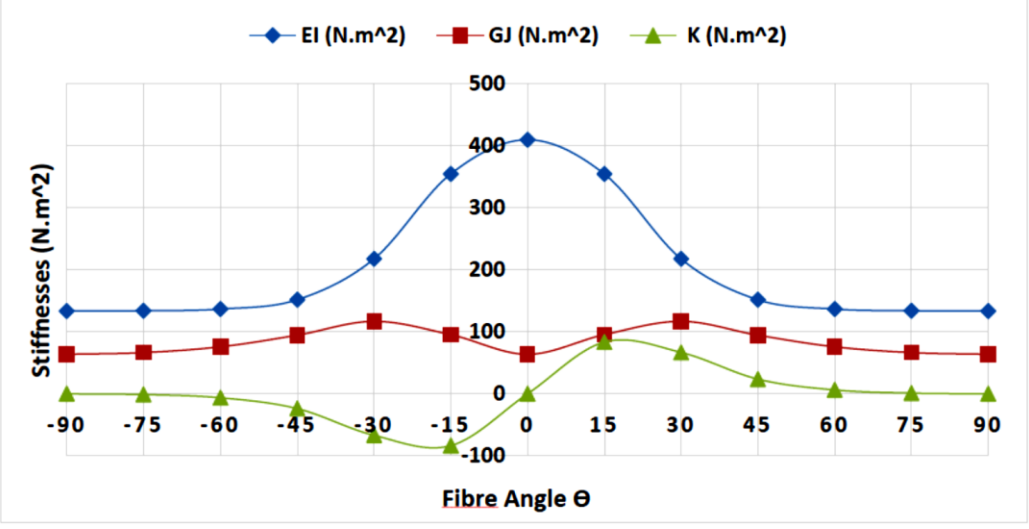

Figure 7: Stiffnesses verse fiber angle Θ, wing 3 model.

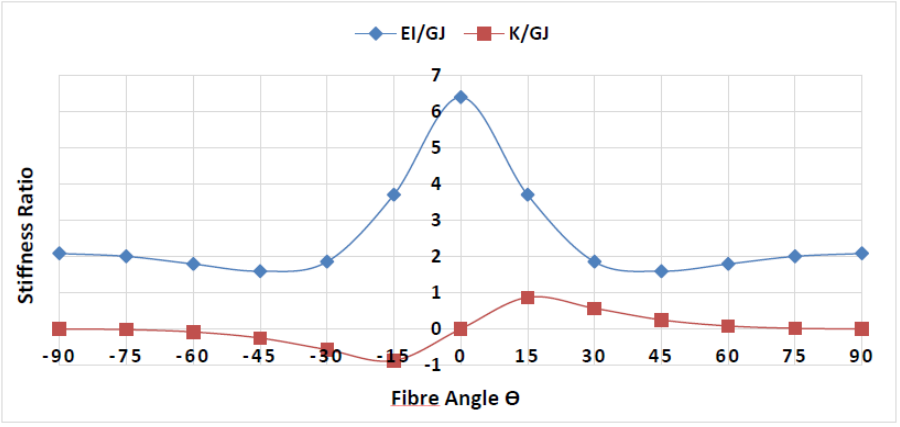

Figure 8: Stiffnesses ratio verse fiber angle Θ, wing 3 model.

Thus, to examine and compare between the wing 1 model and wing 3 model, it can be seen that the stiffnesses of the wing 1 model are slightly higher than the stiffnesses of the wing 3 model, that is due to the effects of the inner angles ply laminate (sequence) θ= 0° and 90° which leads to a higher q_{ij} matrix in wing 1 compared with wing 3 model.

Effect of the Aspect Ratio

The wing aspect ratio in this work is considered as the ratio of the span to the wing chord, and the wing span was taken as constant [11]. There are five values for the aspect ratios $AR = 6, 7, 8, 9$ and 10. The effect of the aspect ratios on the composite stiffnesses and stiffness ratio are considered on wing 1 model, CAS $(\theta_3/0°/90°)_S$ at θ = +45° as shown in Figures (9) and (10).

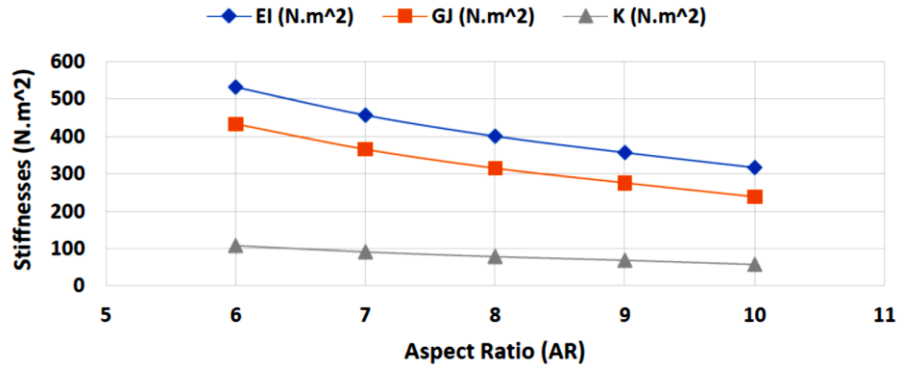

Figure 9: Stiffnesses versus aspect ratio.

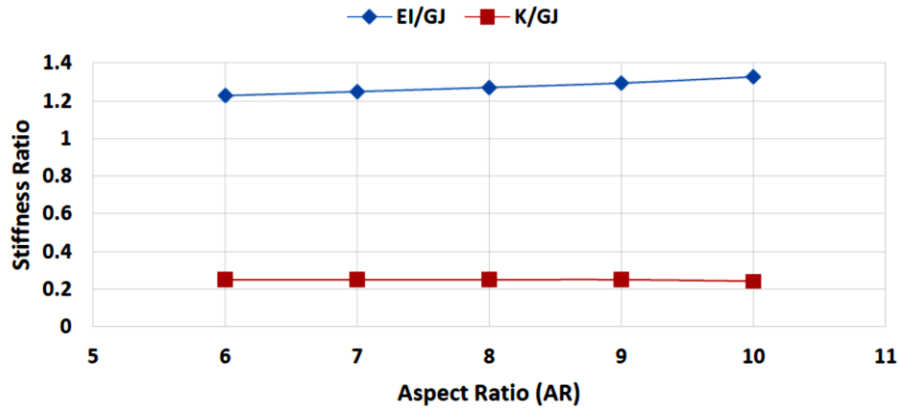

Figure 10: Stiffnesses ratio versus aspect ratio.

From the Figure (9), it can be seen that the maximum stiffnesses (EI, GJ, K) are found at aspect ratio $AR = 6$,then the stiffnesses $(EI, GJ,\ K)$ start decreasing as the aspect ratio increased, this variation leads to increasing of the stiffnesses ratio $^{EI}/_{GJ}$ and $^{K}/_{GJ}$ as the aspect ratio increases as shown in Figure (10), which is due to the effects of the chord.

NORMAL MODE ANALYSIS USING MSC/NASTRAN

Equation of motion

The governing differential coupling equations of motion in free vibration are given by:

$$EI\frac{\partial^4 H}{\partial y^4} + K\frac{\partial^3 \emptyset}{\partial y^3} + m\frac{\partial^2 H}{\partial t^2} - m(x)\frac{\partial^2 \emptyset}{\partial t^2} = 0$$

$$GJ\frac{\partial^2 \emptyset}{\partial y^2} + K\frac{\partial^3 H}{\partial y^3} + m(x)\frac{\partial^2 H}{\partial t^2} - I\frac{\partial^2 \emptyset}{\partial t^2} = 0$$

FE models and method

The dimensions and the composite material properties of the wing's models are given in Table (2). free vibration characteristics, natural frequencies and mode shapes for composite wings are evaluated using the finite element program MSC/NASTRAN v 2004. This was accomplished by applying Sol. 103's normal mode analysis. In order to determine the natural frequency and mode shapes, the Lanczos method was chosen. Accurate calculation of its stiffnesses EI, GJ, and K is necessary for normal modes.

CQUAD4 plate elements with four grid points are used to model the composite wings. There were 480 CQUAD4 plate elements in the finite element model. Forty elements were created along the span, five elements along the chord, and one element in the spar webs in order to achieve this. In order to replicate the cantilevered boundary conditions, which are rather close to the actual fuselage-wing connection, the composite wings are modelled. The purpose of this analysis is to examine how the natural frequencies and mode shapes of both wing structures are affected by the bend-twist coupling stiffness K, fibre orientations θ, laminate stacking sequence, and aspect ratios.

In order to gain and show the experience in using this FE program, a similar wing structure (wing 6) was selected from the open literature, Ref. [12] to validate the obtained results. Wing 6 model of Ref. [12] is simulating a Balanced (CUS) configuration. The laminate in the upper skin, $(30°_2/0)_s$ and lower skin $(-30°_2/0)_s$and spar webs, $(\pm 45°)_2$. The results are obtained, compared and presented in Table (5).

Table 3: Comparison of first bending, second bending and first torsion natural frequencies for Ref. [12].

mode	Present (MSC/NASTRAN)	Ref. [12]	Error in (%)
B_1T	34.532 (Hz)	34.987 (Hz)	1.30%
B_2T	213.39 (Hz)	215.124 (Hz)	0.80%
T_1B	689.85 (Hz)	690.52 (Hz)	0.09%

RESULTS

Four-wing models are then constructed to reach the main objectives of the research. Figure (11) displays the eigenvalues obtained from the composite wing 1 and wing 2 models with cantilevered end conditions.

The eigenvalues result of composite wing 3 and wing 4 models with cantilevered end conditions are shown in Figure (12).

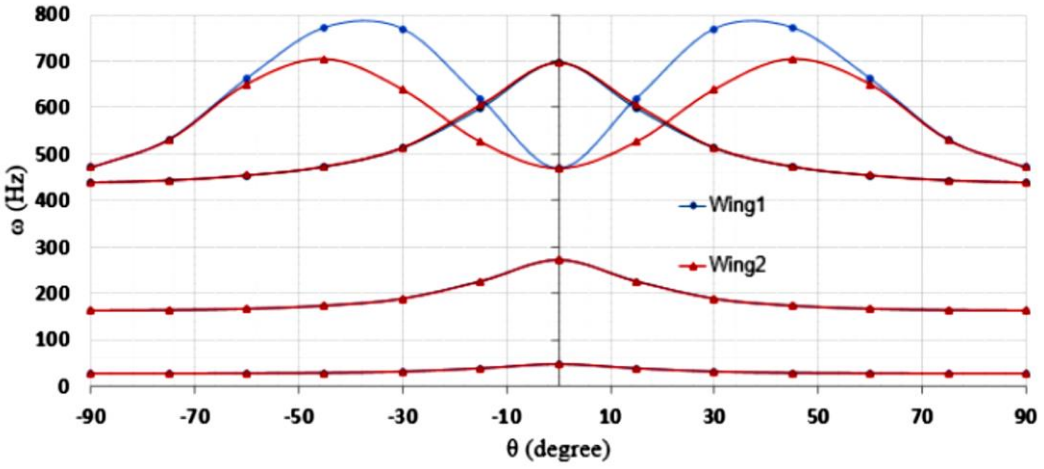

Figure 11: First four bending and torsional frequencies of wing 1 and wing 2 models versus fiber orientation (θ).

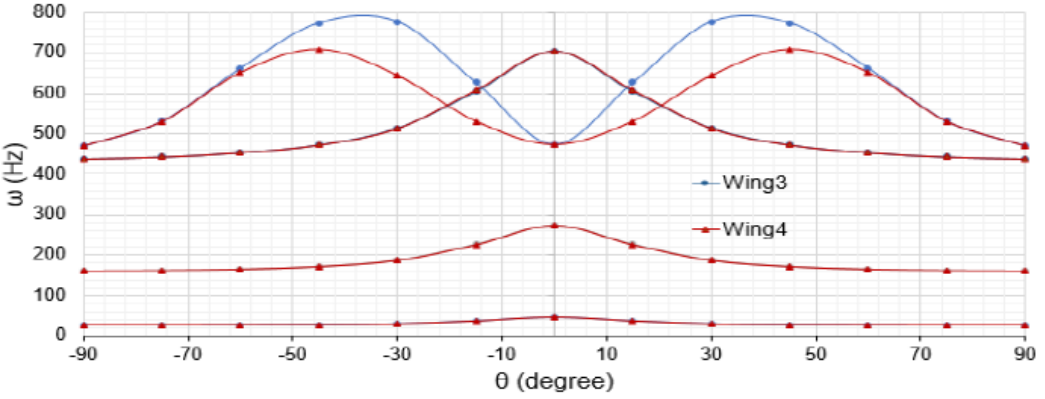

Figure 12: First four bending and torsional frequencies of wing 3 and wing 4 models versus fiber orientation (θ).

Figures (13) to (18) display the results for the Wing 1 model's first six eigenvalues and eigenvectors at θ = 15°.

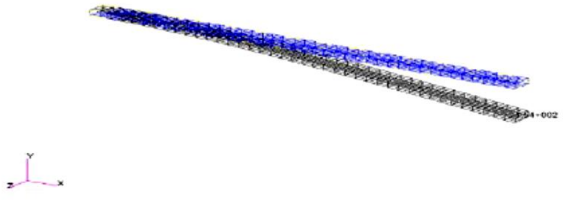

Figure 13: 1st Bend-Twist mode (37.013 Hz), wing 1 at θ = 15°

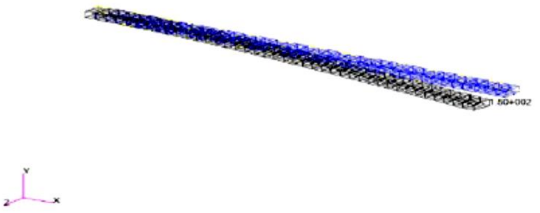

Figure 14: 1st Chord wise mode, (61.829 Hz), wing 1 at θ = 15°.

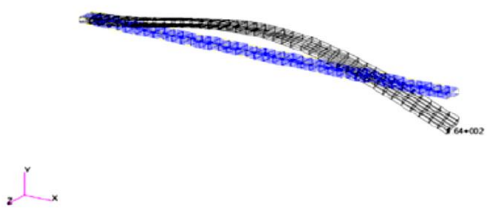

Figure 15: 2nd Bend-Twist mode (225.8 Hz), wing 1 at θ = 15°.

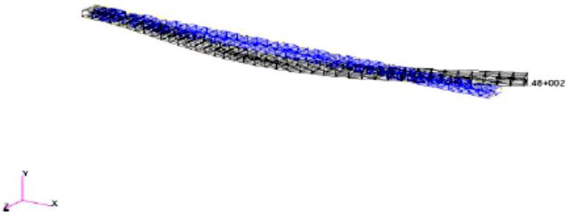

Figure 16: 2nd Chord wise mode (374.74 Hz), wing 1 at θ = 15°

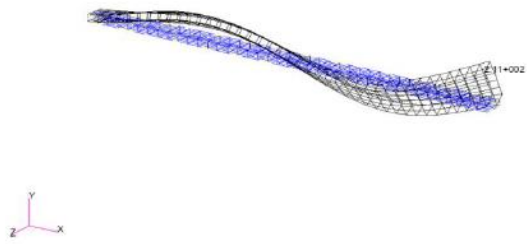

Figure 17: 3rd Bend-Twist mode (598.36 Hz), wing 1 at θ = 15°.

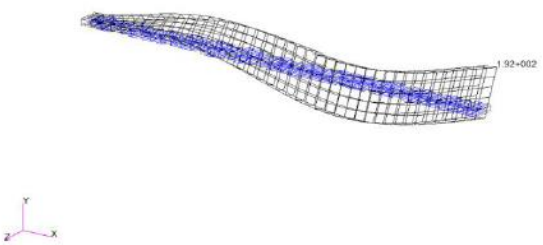

Figure 18: 1st Twist-Bend mode (620.1 Hz), wing 1 at θ = 15°.

Effect of the Aspect Ratio

Practical and realistic values of aspect ratio (AR) in aircraft wing structures are very important and considered in this research, as it changes the dimensions of the wing and as a result will change the stiffnesses and masses of the wing structure. This will affect the vibration and flutter behaviours of composite wing configurations. The effect of the aspect ratio on the natural frequencies is considered on wing 1 model, CAS $(\theta_3/0°/90°)_S$ at θ = +45° as shown in Figure (19).

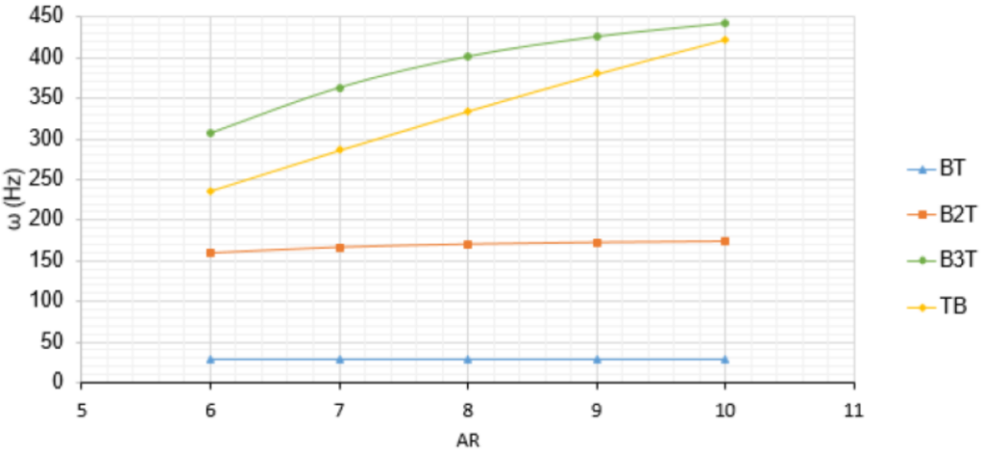

Figure 19: First four bending and torsional frequencies of wing 1 model versus AR at θ = +45⁰.

DISCUSSION OF RESULTS

As shown in Figures (11) and (12), wing 1 and wing 3 models (CAS), the modes shape changes are observed with ply angle orientation for 0° ≤ θ ≤ ±45°. The first mode is characterized as a fundamental bending with a small torsion displacement for 0° < θ ≤ ±45°. The first mode shape at θ = 0° and 90° are purely bending modes. The third mode is basically a dominated second bending with a small torsion displacement for 0°< θ ≤ ±45° and were purely bending modes at θ = 0° and 90°. At θ = 0°, the fifth mode is pure fundamental torsion and the sixth mode is basically a dominated pure third bending. Where 0° <θ< ±90°, the sixth mode is fundamental torsion with a small bending displacement, but with a clear mode at 90° and the fifth mode is third bending with a small torsional displacement except at 90°.

When looking at Figures (11) and (12) for wing 2 and wing 4 models, the first mode is pure fundamental bending mode for 0° ≤ θ ≤ ±90°, (K=0) in the case of (CUS). The third mode is purely second bending modes for all values of θ. When θ ≤ 15°, the fifth mode is pure first torsion mode and sixth mod is purely third bending mode, but at θ >15°, fifth mode is third bending mode and the sixth mode is first twisting mode.

Comparing the results of wing 1 (CAS) and wing 2 (CUS) models, it was observed that the first three bending frequency modes of wing 1 model are slightly higher for $0° < \theta < \pm 90°$ compared with wing 2 model and equal at $\theta = 0°$ and $\pm 90°$, due to the presence of material bend-twist coupling stiffness in wing 1 model, see Figure (11).

The effect of material coupling on the torsional eigenvalue as in the case of wing 1 and wing 2 models is more pronounced on the torsional frequency. After close inspection in the Figure (11), it was found that torsional frequencies of wing 1 model higher than the wing 2 model especially where the coupling was higher. The maximum torsional frequency is occurred at $\theta = \pm 45°$ for both wing models and then start decreasing as the fibre angle increased.

For wing 3 (CAS) and wing 4 (CUS) models, it was found that the same behaviour as in wing 1 and wing 2 models is observed in the first bending, second bending and third bending natural frequencies modes, but different in the torsional frequency. The torsional frequency of wing 3 is higher than the wing 4 model due to the effect of the coupling, (K). The maximum torsion frequency occurred at $\theta = \pm 30°$ for wing 3, which was not the case of wing 1 model and at $\theta = \pm 45°$ for wing 4 modal. This is could be due to the sequence of the plies with respect to the reference line of the laminate as θ is very close to the line compared to the wing 1 model. It can be said that having the fibre angle θ in the inner plies as in wing 3 model is more beneficial to the torsional frequency.

It was noticed that, the effect of bend-twist coupling stiffness (K) on the bending frequency was almost negligible as in the case of CAS wing models especially at higher values of K.

It can be seen that the effect of laminate stacking sequence on natural frequencies and mode shapes between wing 1 and wing 3 models for the first bending, second bending, third bending and first torsional natural frequencies, is that the wing 3 model slightly higher than the wing 1 model due to the inner ply angles $(90°/0°/\theta_3)_s$.

The effect of aspect ratio on the eigenvalues and associated eigenvectors was illustrated in Figure (19). The first bending, is almost constant for all aspect ratios. The second and third bending modes are slightly increasing when the aspect ratio increases and the third mode is characterized as the first torsion mode, increases as the aspect ratio increases.

CONCLUSIONS

In this study, four wing models are constructed from two thin-walled structures as presented in Figures (2) and (3) which are simulated Circumferentially Asymmetric Stiffness (CAS) and Circumferentially Uniform Stiffness (CUS). A computer program using MATLAB language is developed to calculated the effective bending stiffness EI, torsion stiffness GJ, and material coupling stiffness K, using the method derived by Chandra et al. Ref. [6]. Through the use of Solution 103 for normal mode analysis utilizing the Lanczos method, the free vibration properties of composite wing models have been thoroughly investigated using MSC NASTRAN. The following conclusions are compiled and given as a result of the analysis done for all wing models in this study:

- The torsional frequency increased in comparison to the CUS wing models when the bending-torsional coupling stiffness was excluded, as was the case with the CAS wing models when the bending-torsional coupling stiffness was included.
- There was very little change in the bending frequency due to bending-torsional coupling. On the other hand, in the case of CAS wing models, the effect of

material coupling on the mode shapes was more apparent particularly in the region of increased coupling stiffness.

- The natural frequencies and mode shapes of the wing 1 and wing 3 models were affected by the laminate stacking sequence. The wing 3 model's natural frequencies, $(90°/0°/\theta_3)_S$, are greater than those of the wing 1 model because of the inner ply angles.
- Aspect ratio had a noticeable and proportional impact on natural frequencies and mode shapes in relation to the first torsional frequency, but it had a minor effect on the first bending frequency.

LIST OF SYMBOLS

Symbol	Definition
CAS	Circumferentially Asymmetric Stiffness
CUS	Circumferentially Uniform Stiffness
MSC	MacNeal-Schwendler Corporation
NASTRAN	NASA STRucture ANalysis.
E_1	longitudinal young's modulus in direction 1
E_2	transverse young's modulus in direction 2
v_{12}	major Poisson's ratio
G_{12}	in-plane shear modulus in plane 1–2
θ	ply angle
q_{ij}	transformed reduced stiffness
EI	bending stiffness
GJ	torsion stiffness
K	coupling stiffness
AR	Aspect Ratio
B_1T	first bending mode with torsion displacement
B_2T	second bending mode with torsion displacement
T_1B	first torsion mode with bending displacement
ρ	density
m	mass per unit length
I	mass moment of inertia per unit length
x	distance between shear center and mass center
H(y, t)	bending displacement
∅(y, t)	torsional rotation

REFERENCES

[1] Bisplinghoff, R. L., Ashely, H. and Halfman, R. L., (1996), "Aeroelasticity". Dover Publications, INC., Mineola, New York.

[2] Vo, T. P., and Lee, J., (2009)," Free Vibration of Thin-Walled Composite Box Beams", Architectural Engineering, Sejong University.

[3] Khan, J. Z., (1992), "Static, Dynamic and Aeroelastic Behaviour of Thin-Walled Composite Structures with Application to Aircraft Wings ", DSc Thesis, Department of Mechanical Engineering and aeronautics, City University.

[4] Ovesy, H. R., and Masjedi, P. K., (2014), "Investigation of the Effect of Constitutive Equations on the Free Vibration Behaviour of Single-Celled Thin-Walled Composite Beams", Mechanical of Advanced Materials and Structures, 21, 836-852.

[5] Banerjee, J. R. and Williams, F. W., (1995)," Free vibration of composite beams- an exact method using symbolic computation". Journal of Aircraft, vol. 32, no. 3.

[6] Sari, B., Kazemi Lichaei, M., and Yildirim, S., (2022), "Free Vibration Analysis of Tapered Composite Aircraft Wing via the Finite Element Method", Cukurova University Journal of the Faculty of Engineering, 37(3), pp. 741-752.

[7] Clydin, P. A. and Nithin, M., (2017), "Free Vibration of Laminated Composites Beams Using Strain Gradient Notation Finite Element Model", International Journal of Engineering Research & Technology (IJERT), ISSN: 2278-0181, Vol. 6 Issue 12.

[8] Hortaa, T.B. and Filho, J. E., (2021), "Free Vibration of Laminated Composites Beams Using Strain Gradient Notation Finite Element Models", Materials Research, 24(suppl. 2): e20210394.

[9] Chandra, R., Stemple, A. D., And Chopra, I., (1990), "Thin-Walled Composite Beams Under Bending, Torsion, And Extensional Loads", Journal of Aircraft, Vol. 27, pp.626.

[10] Georghiades, G. A., (1997), "Aeroelastic Behaviour of Composite Wings", Ph.D. Thesis, City University.

[11] Lee, I. and Lee, J. J., (1990), "Vibration Analysis of Composite Plate Wing". Computers and Structures, Vol.37, No.6, pp.1077-1085.

[12] Ashawesh, G. M., (1999), "Flutter Behaviour of Composite Aircraft Wings", Ph.D. Thesis, Cranfield University.